Available online at www.sciencedirect.com
SCIENCE DIRECT®
Journal of Solid State Chemistry 177 (2004) 3490–3498
JOURNAL OF SOLID STATE CHEMISTRY
http://elsevier.com/locate/jssc

Significant effect of lanthanide doping on the texture and properties of nanocrystalline mesoporous TiO_2

Yuhong Zhang,* Huaxing Zhang, Yongxi Xu, and Yanguang Wang

Institute of Inorganic Chemistry, Department of Chemistry, Zhejiang University, Hangzhou 310028, China

Received 7 February 2004; received in revised form 10 May 2004; accepted 13 May 2004

Available online 11 August 2004

Abstract

A systematic study of microstructure and photocatalytic properties of lanthanide doping of nanocrystalline mesoporous titanium dioxide is performed. The anatase-to-rutile (A-R) phase transformation of nanosized TiO_2 was significantly inhibited by lanthanide doping and the inhibitory effect was enhanced with the increase of the rare earth radius, i.e., $La^{3+} > Gd^{3+} > Yb^{3+}$ for different lanthanide dopants. At high calcination temperatures, different texture lanthanide titanium oxides of $Ln_4Ti_9O_{24}$ (La^{3+}, Pr^{3+}, Nd^{3+}), $Ln_2Ti_2O_7$ (Eu^{3+}, Gd^{3+}, Tb^{3+}, Dy^{3+}, Er^{3+}), and Yb_2TiO_5 were developed, respectively, revealing that the structures of lanthanide titanium oxide developed in Ln/TiO_2 depend on the lanthanide radius. Larger radius lanthanides prefer to form higher coordination number lanthanide titanium oxide. In addition, the thermal stability of mesoporous structures of TiO_2 was remarkable improved by lanthanide doping. The photocatalytic properties were studied by employing the photodegradation of Rhodamine B (RB) as a probe reaction. The results indicate that the lanthanide doping could bring about significant improvement to the photoreactivity of TiO_2, and the improvement was sensitive to the atomic electronic configuration.

Keywords: Lanthanide dopants; Titania; Phase transformation and photocatalytic property

1. Introduction

Titanium dioxide is an important catalyst and catalyst support [1]. In particular, the photocatalytic properties of titanium dioxide were extensively investigated due to its high light-conversion efficiency, high stability toward photocorrosion, and environmental benign properties [2–4]. It has been widely demonstrated that the photocatalytic reactivity of titanium dioxide is sensitive to its microstructures [5–7]. For example, anatase shows a better performance than rutile in the photocatalysis [8,9]; quantum sized TiO_2 powders possess larger specific surface areas and are expected to have good catalytic activities since reactions take place on the TiO_2 surface [10]. However, nanosized TiO_2 undergoes an earlier phase transformation of anatase-to-rutile (A-R) than its bulk phase, and is companied with a great diminishing of surface area at relatively low temperatures. Numerous investigations are devoted to the modification of microstructures and improvement of reactivity of nanosized TiO_2 [11–13].

Doping metal ions in TiO_2 has been proven to be an efficient route to alter both the photoactivity and A-R phase transformation of nanosized titania [14–20]. The suitable metal ion dopant appears to be the most important factor in the enhancement of photoreactivity of doped titania [21–25]. Recently, doping lanthanide into TiO_2 attracted many attentions [26–31]. Lanthanide ions are known for their ability to form complexes with various Lewis bases (e.g., acids, amines, aldehydes, alcohols, thiols, etc.) in the interaction of these functional groups with the *f*-orbitals of the lanthanides. Thus, incorporation of lanthanide ions into a TiO_2 matrix could provide a means to concentrate on the organic pollutant at the semiconductor surface and therefore enhance the photoactivity of titania [32–35]. With the objective to understand the effect of lanthanide dopants better, we systematically studied the lanthanide-doped nanocrystalline mesoporous TiO_2. It

*Corresponding author. Fax: +86-571-8795-1895.
E-mail address: yhzhang@zjuem.zju.edu.cn (Y. Zhang).

0022-4596/$ - see front matter © 2004 Elsevier Inc. All rights reserved.
doi:10.1016/j.jssc.2004.05.026

is discovered that the radius and atom structure of the lanthanides have a great influence to the development of inhibitory efficiency of A-R transformation, development of lanthanide titanium oxide and the photoreactivity of TiO_2. Three series were presented here: lanthanum-, gadolinium-, and ytterbium-doped TiO_2, in which the atomic/ionic radius of the lanthanides is gradually decreased. An easy sol–gel technique reported earlier for the preparation of homogeneously ion-doped titania was used [21]. The phase transformation and sintering process studies combined with the photoreactivity tests here will provide insights into the effects of rare earth doping on the texture and photocatalysis of TiO_2.

2. Experimental section

2.1. Preparation of samples

The lanthanide-doped titania were prepared by an easy sol–gel technique reported else where [21]. The typical procedure for the preparation of lanthanide-doped titania is given below: commercial stoichiometric oxide lanthanide (99.9%, ACROS) was dissolved in a minimum amount of nitric acid and then evaporated to dryness. Butanediol (2 g) and tetrabutyl-orthotitanate (98%, ACROS, 3 g) was added into the dry lanthanide nitrate powder under magnetic stirring at room temperature until a homogeneous transparent solution resulted. The solution is very stable and can be stored for over one year in the sealed bottle without coagulation. Exposing the solution in air at room temperature for one week, a dry solid gel resulted, which is further heated at 120°C for 5 h. The doped nanocrystalline was finally obtained by heating the dry solid gel at different temperatures above 400°C for 1 h in air using a Naber 7H furnace. The heating program is 3°C/min for each sample. The samples containing 0, 0.25, 0.5, 1, 2, 3, and 5 at% lanthanum are labeled as LT0, LT1, LT2, LT3, LT4, LT5, and LT6. The samples containing 0, 0.25, 0.5, 1, 2, 3, and 5 at% gadolinium are labeled as GT0, GT1, GT2, GT3, GT4, GT5, and GT6. The same content ytterbium-doped samples are labeled as YT0, YT1, YT2, YT3, YT4, YT5, and YT6. All the dopant concentrations mentioned in this work are the atomic concentration.

2.2. Photocatalysis measurements

The Rhodanmine B dye was of laser grade. Deionized water was used throughout the experiment. The photoactivity of each doped TiO_2 system is detected by the photodegradation of Rhodamine B at ambient temperature. Irradiation was performed with a 300 W, 365 nm UV lamp (Institute of Electric Light Source, Shanghai, China) surrounded by a circulating water jacket (Pyrex) to cool the lamp. For each irradiation experiment, 50 mg as prepared catalyst of *Ln*–TiO_2 was added to a 25-mL aqueous solution containing RB dye ($C_0 = 10^{-5}$ M), and for each irradiation it was carried out for 30 min. The distance between UV lamp and reactor is 30 cm for each experiment. After irradiation and removal of the *Ln*–TiO_2 particles by centrifugation and filtration, the filtrates were analyzed by a Shimadzu UV-2000 spectrophotometer.

2.3. Characterization

N_2 adsorption/desorption isotherms of the samples were carried out at liquid N_2 temperature in an Omnisorp 100CX instrument. The specific surface areas were calculated by the BET equation. The pore size distribution was determined by desorption branches. The study of crystal and the structure/modification of the products were performed on a Bruker D8 X-ray diffractometer using Cu$K\alpha$ radiation. The identification of crystalline phases was accomplished by comparison with JCPDS files numbered as 21-1272, 21-1276, 83-946, 23-259, and 33-1457 for anatase, rutile, lanthanum titanium oxide ($La_4Ti_9O_{24}$), gadolinium titanium oxide ($Gd_2Ti_2O_7$), and ytterbium titanium oxide (Yb_2TiO_5), respectively. The average crystal size of the doped samples was calculated from the anatase peak broadening (101 crystal plane with Scherrer's equation). The investigation of the particle morphology and microstructure was performed on a JEM-200CX transmission electron microscope (TEM) and the micrographs were recorded at 300 kV.

3. Result and discussion

Three series of homogeneously lanthanide-doped nanocrystalline titania samples were successfully produced. At the beginning of the preparation, lanthanide nitrate and titanium isopropoxide precursor were homogeneously dissolved in butanediol and a uniform transparent solution formed. This solution is very stable and can be stored for over one year in a sealed bottle without coagulation because no acid, water, or alcohol are introduced. The subsequent sol–gel process took place for a week in the air and the homogeneous dispersion of Ln^{3+} is further consolidated by heating at 120°C for 5 h. Lanthanide-doped nanocrystalline titania was finally obtained by heat treatment above 400°C. In our experiment, the deposition of lanthanide oxide on the surface of titania particles happened in the impregnation method is avoided and the dispersion of lanthanum oxide particles within the freshly precipitated titanium dioxide particles by co-precipitation is prevented effectively. Thermogravimetric analysis showed

that 90% of the weight loss takes place below 300°C and the weight loss is completed at 450°C, implying that the organic composition is totally burned away.

Fig. 1 presents the XRD results of lanthanum-doped titania calcined at 800°C and 900°C for 1 h in air. It is seen that the anatase phase at high temperatures is remarkably stabilized by lanthanum doping. The transformation of A-R of pure as-prepared nanosized TiO_2 took place between 630°C and 730°C. Thus the pure as-prepared TiO_2 only shows a single rutile phase in Fig. 1A. It should be noted that the anatase is maintained for 0.25% lanthanum-doped sample calcined at 800°C, demonstrating that lanthanum doping has a significant inhibitiory effect to the A-R phase transformation. It is manifest that this remarkable shift of the phase transformation to high temperatures is caused by the lanthanum doping. It is expected that the surrounding lanthanum ions will inhibit the phase transition of A-R through the formation of Ti–O–La bond. On the other hand, the La_2O_3 lattice locks the Ti–O species at the interface with the TiO_2 domains preventing the nucleation that is necessary for anatase transformation to rutile.

When the calcination temperature was increased to 900°C (Fig. 1B), the significant changes take place. LT1 (0.25%) and LT2 (0.5%) samples show a mixture phase of anatase and rutile, and the relative ratio of R/A is reduced with the increase of lanthanum content. Further increasing lanthanum content to 1% (LT3), no rutile reflection was observed and a single anatase phase was retained. It should be noted that the rutile reflections appeared when the lanthanum content increased to 3% (LT5), inferring a reduction of A-R phase transition temperature. In LT6 (5%) the relative ratio of R/A is enhanced continuously. It is manifest that the optimum inhibitory effect is obtained by 1% lanthanum-doped sample. The similar result is observed by other rare earth-doped titania [35]. The mechanism for this change is possibly related to the formation of $La_4Ti_9O_{24}$ and enhancement of defects for high lanthanide content samples [36].

The phase transformation of gadolinium- and ytterbium-doped titania is illustrated in Figs. 2 and 3, respectively. Even though the phase transformation of

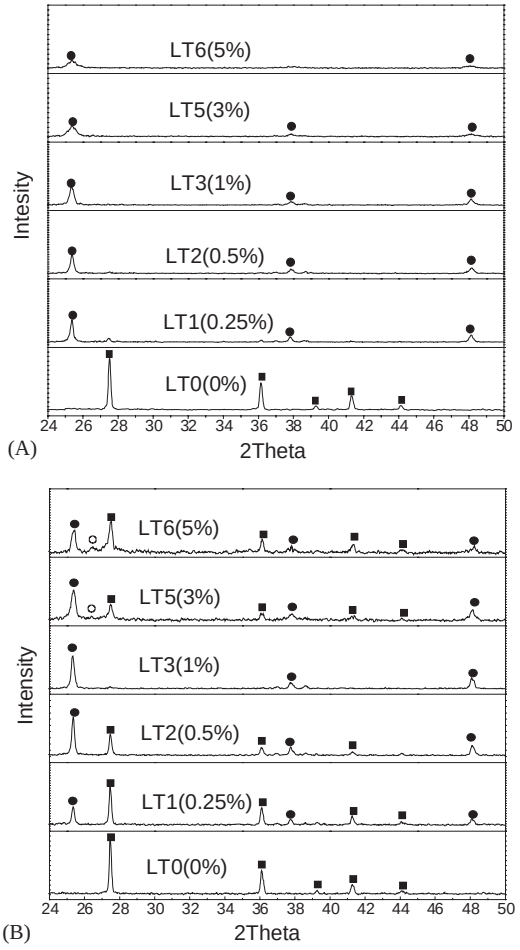

Fig. 1. XRD diffraction patterns of lanthanum-doped titania samples calcined at 800°C (A) and 900°C (B) for 1 h in air. (■): rutile; (•) anatase; (○): lanthanum titanium oxide ($La_4Ti_9O_{24}$).

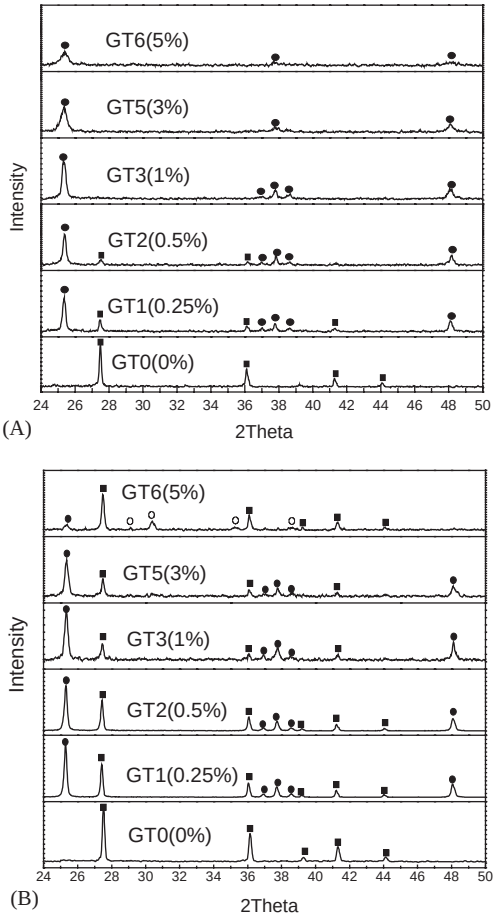

Fig. 2. XRD diffraction patterns of gadiolium-doped titania samples calcined at 800°C (A) and 900°C (B) for 1 h in air. (■): rutile; (•): anatase; (○): gadolinium titanium oxide ($Gd_2Ti_2O_7$).

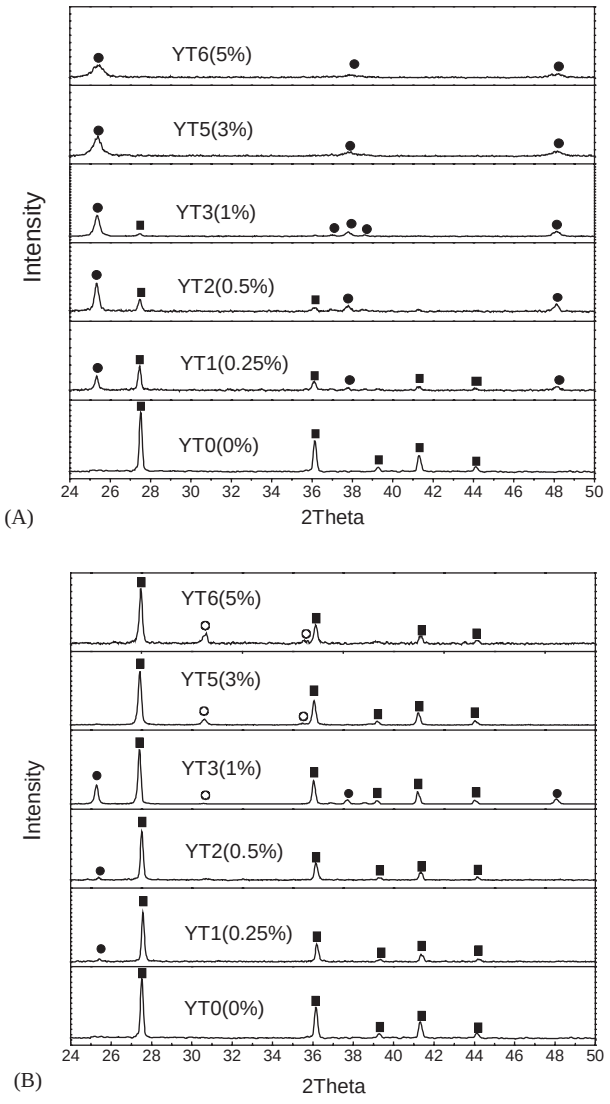

Fig. 3. XRD diffraction patterns of ytterbium-doped titania samples calcined at 800°C (A) and 900°C (B) for 1 h in air. (■): rutile; (●): anatase; (○): ytterbium titanium oxide (Yb_2TiO_5).

gadilinium- and ytterbium-doped titania is very similar with lanthanum-doped samples, the degree of inhibition to the A-R transformation is different. The XRD patterns of lanthanum-, gadolinium-, and ytterbium-doped titania calcined at 800°C for 1 h in air were showed in Figs. 1A, 2A and 3A, respectively. It is seen that only LT1 (0.25%) is displayed a small rutile peak at about 27.52° 2θ in lanthanum-doped TiO_2. In the gadolinium-doped samples (Fig. 2A), the development of rutile phase is observed in both GT1 (0.25%) and GT2 (0.5%), and the relative ratio of rutile/anatase in GT1 is obviously enhanced when compared with the same concentration lanthanum-doped sample LT1. The development of rutile modification is further extended to YT3 (1%) (Fig. 3A) in the ytterbium-doped system, and the rutile becomes the main phase in YT1 (0.25%). The variation in A-R phase transformation temperature suggests that the sequence of the retarding effect on the A-R transformation by the additives is: $La^{3+} > Gd^{3+} > Yb^{3+}$, i.e., the inhibitory effect of lanthanide-doped titania is sensitive to the lanthanide ionic radii.

This trend is even more obvious in the lanthanide-doped samples calcined at 900°C. The XRD patterns of lanthanum-, gadolinium-, and ytterbium-doped titania calcined at 900°C for 1 h in air were presented in Figs. 1B, 2B and 3B, respectively. It is seen from Fig. 3B that the ytterbium-doped samples is nearly complete the A-R phase transformation and the rutile is the main modification, while a substantial amount of anatase is still left over in the lanthanum-doped samples (Fig. 1B), and the A/R ratio depends on the lanthanum concentration. The maximum inhibitory effect is achieved in LT3 (1%), which still maintained a single anatase modification. Further increasing of lanthanum content causes the reduction of the anatase/rutile ratio. In gadolinium-doped samples, neither a single anatase nor a single rutile modification can be observed. The inhibition effect of same content gadolinium-doped samples is between that of lanthanum and ytterbium-doped samples. This variation of inhibitory effect for different lanthanides is probably connected to the lanthanide contraction. The ionic radii of the lanthanide is: La^{3+} (0.104 nm) > Gd^{3+} (0.094 nm) > Yb^{3+} (0.081 nm) because of the lanthanide contraction. When the calcination temperature was raised to a level allowing the A-R transformation, due to the mismatch of the ionic sizes of Ti^{4+} and Ln^{3+}, the lanthanides substituting for Ti^{4+} are probably expelled into the interstitials and existed as amorphous oxide lanthanide, which will react with rutile to form lanthanide titanium oxide further. Likely, the larger radius Ln^{3+} is easier to be expelled and more difficult to form lanthanide titanium oxide. This means that in the A-R transition process the larger radius lanthanides have more chance to be existed as amorphous oxide lanthanides in the interstitials, which will block the nucleation of rutile and inhibit the A-R phase transformation. In contrast, the easier formation of lanthanide titanium oxide, as we discussed before, is probably favorable to the A-R phase transformation. The similar result was observed in the study of A-R phase transformation by Lin et al. in a mixture of TiO_2 and oxide lanthanides [33]. In their work, the XRD results revealed that even with a moderate thermal treatment (650–700°C), the presence of the oxide lanthanide could inhibit the A-R phase transformation. In the silicon-doped titania, silicon exhibits significant inhibition effect to the A-R phase transition and silicon titanium oxide is difficult to be formed due to the mismatch of their ionic radii (Si^{4+} = 0.040 nm, Ti^{4+} = 0.061 nm) [20,37].

The lanthanium titanium oxide ($La_4Ti_9O_{24}$), gadolinium titanium oxide ($Gd_2Ti_2O_7$), and ytterbium titanium oxide (Yb_2TiO_5) are evolved in the three lanthanide-doped titania samples, respectively, after the heat treatment of 900°C for 1 h in air. The evolution of lanthanide titanium oxide, unlike the inhibition efficiency at high temperatures, is proportional to the lanthanide content. The intensity of lanthanide titanium oxide peak is gradually increased with the enhancement of lanthanide content (Figs. 1B, 2B and 3B). The detailed analysis of XRD patterns for the identification of the lanthanide titanium oxide crystal structures are made as shown in Fig. 4. It can be seen from Fig. 4A that some new reflections are appeared at 26.42°, 26.64°, 27.13°, 27.93°, 28.08°, 30.13°, 31.45°, 35.07°, 35.34°, 45.35°, 45.70°, 45.82°, 50.02°, 50.21°, 51.04°, 51.16°, 52.91°, and 47.82° 2θ, owing to the reflections of $La_4Ti_9O_{24}$ (face centred orthorhombic). Unlike lanthanum-doped titania samples, $Gd_2Ti_2O_7$ (face centred cubic) is developed at high heat treatment temperatures in the gadolinium-doped titnia showing in Fig. 4B. In the ytterbium-doped titania samples calcined at 900°C, well resolved new peaks are observed at 30.70°, 35.59°, 51.10°, and 60.74° 2θ. Comparing these reflections with JCPDS standard data of $Yb_2Ti_2O_7$ (29.548°, 30.910°, 35.883°, 39.137°, 47.063°, 51.545°, 54.095°, 61.306°, and 64.336° 2θ) and Yb_2TiO_5 (30.262°, 35.159°, 50.637°, 60.157° 2θ), we concluded that a distorted face centred cubic Yb_2TiO_5 was developed in the ytterbium-doped titania. The XRD results of other lanthanide-doped TiO_2 revealed that face centred orthorhombic ($Ln_4Ti_9O_{24}$) in Pr^{3+}-, Nd^{3+}-doped TiO_2 and face centred cubic ($Ln_2Ti_2O_7$) in Eu^{3+}-, Gd^{3+}-, Tb^{3+}-, Dy^{3+}-, Er^{3+}-doped TiO_2 were formed. The evolution of various lanthanide titanium oxides is manifested in the dependence of their ionic radii. Due to the lanthanide contraction, the atom/ionic radius is decreased with the increase of the atomic number in lanthanides. The ionic radius of these lanthanides is as follows: $La^{3+} > Gd^{3+} > Yb^{3+}$. Because the anion ligand O^{2-} is same in the lanthanide-doped titania, the coordination number, and hence the structure, is determined by lanthanide ions' size. The characteristic coordination numbers of lanthanide decrease with rise in atomic number, i.e., reduction of atomic radius.

From the broadness of the anatase peak (101), the average crystallite sizes of the lanthanide-doped titania calcined at 700°C for 1 h in air were calculated (Table 1) by Scherrers' equation [38]. Obviously, the lanthanide-doped samples have finer crystallites than undoped titania. The average crystallite size was 56.42 nm for undoped titania, while a considerable reduction in size was observed after doping with 1% lanthanides. With the increase of lanthanide dopant content, the average crystallite size progressively decreased. This reduction in crystallite size is proposed to be due to segregation of the dopant cations at the grain boundary, which inhibits the grain growth by restricting direct contact of grains [35]. Ytterbium, lanthanum and gadolinium dopants show the similar inhibitory effect to the grain growth of nanosized TiO_2.

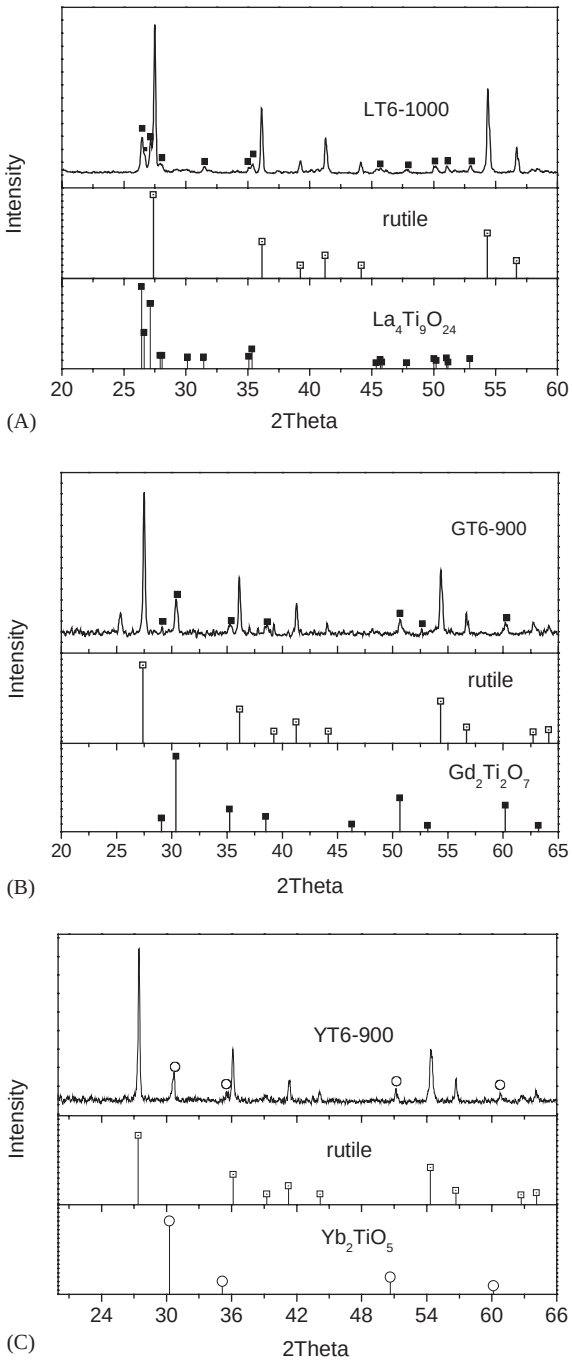

Fig. 4. XRD diffraction patterns of different lanthanide titanium oxides in various lanthanide-doped titania calcined at high temperatures for 1 h in air. (A) LT6 (5 at% lanthanum) calcined at 1000°C. (B) GT6 (5 at% gadolinium) calcined at 900°C. (C) YT6 (5 at% Ytterbium) calcined at 900°C.

To access the size and morphology of the lanthanide-doped titania particles, we performed transmission

Table 1
Average grain size of the lanthanum (LT), gadolinium (GT), and ytterbium (YT) doped titania calcined at 700°C for 1 h in air by Sherrer's equation

Lanthanide content (at%)	0	0.25	0.5	1	2	3	5
LT-700 (nm)	56.42	23.8	20.7	14.5	13.3	12.2	11.9
GT-700 (nm)	56.42	27.6	24.5	18.5	14.6	12.7	11.6
YT-700 (nm)	56.42	25.4	21.1	14.9	13.2	12.9	11.9

electron microscopy (TEM). Fig. 5 presents the TEM micrographs of LT6, GT6, and YT6 heated at 700°C for 1 h in air. It can be seen that the particle size of the lanthanide-doped titania is uniform and the average diameter is around 12 nm. The results are consistent with the XRD analysis (as shown in Table 1), further confirming that the sintering process of titania nanoparticles at high temperature is effectively retarded by lanthanide dopants.

Table 2 lists the BET surface area and pore size of several pure and lanthanum-doped TiO_2 calcined at 500°C and 700°C for 1 h in air. According to the results of Table 2, the BET surface area of the samples was strongly dependent on the lanthanide content and thermal treatment temperatures. It is seen that the surface area of both pure and doped samples is decreased when the temperature is increased from 500°C to 700°C. Heavy densification took place in the undoped TiO_2 at 700°C, which induces the drastic surface area decreasing (0.07 m^2/g). It is worth to note that the surface area of 0.25% lanthanum-doped sample prepared at the same condition is increased to 17.13 m^2/g, implying that the lanthanide dopants have a significant inhibitory effect to the sintering of nanosized TiO_2. Concerning the other doped samples calcined at 700°C, it is observed that their surface areas are progressively increased with the enhancement of the lanthanum content, which is obviously caused by the crystallite size reduction (Table 1). Analogous results were obtained from ytterbium and gadolinium-doped TiO_2.

The as-prepared samples calcined below 500°C for 1 h in air showed the mesoporous structures with narrow pore size distributions. However, when the calcination temperatures further increased, the nanocrystalline mesoporous structure of bare titania corrupted progressively, which might be ascribed to the strong densification of the TiO_2 matrix. It is important to note that the thermal stability of the titania was significantly increased by lanthanide doping. Fig. 6 displays the nitrogen adsorption–desorption isotherms (Fig. 6A) and the pore size distribution (Fig. 6B) of some doped samples calcinated 700°C for 1 h in air. The isotherms of LT1 (0.25%), LT4 (2%), LT5 (3%), and LT6 (5%) calcined at 700°C show a type IV isotherm and H2

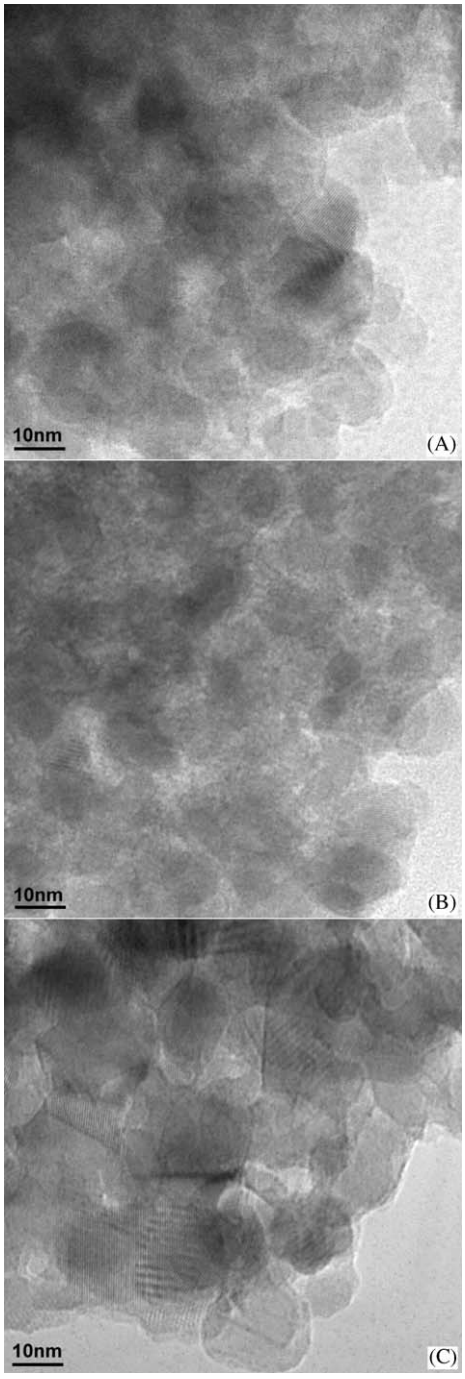

Fig. 5. TEM micrographs of lanthanide-doped titanium dioxide calcinated at 700°C for 1 h by using the same heating program in air. (A) LT6 (5 at% lanthanum) (B) GT6 (5 at% gadolinium) and (C) YT6 (5 at% ytterbium).

hysteresis. The big hysteresis is attributed to the existence of pore cavities larger than the openings (throats), leading ink-bottle pores [39]. The steepness of desorption branch indicates the uniformity in diameter of the throats, which is attributed to the specific synthesis method followed in this route. Narrow pore distributions are observed for the lanthanum-

Table 2
Surface area and pore size of pure and lanthanum doped TiO_2 samples calcined at 500°C and 700°C for 1 h in air

Sample	$T = 500$°C			$T = 700$°C		
	S ($m^2 g^{-1}$)	PS (nm)	Phase	S ($m^2 g^{-1}$)	PS (nm)	Phase
LT0	17.41	3.7	a	0.08	—	r, a
LT1	35.26	3.8	a	17.138	—	a
LT4	96.03	1.9	a	40.95	4	a
LT5	100.13	1.8	a	41.90	4	a
LT6	105.56	1.7	a	45.28	3.8	a

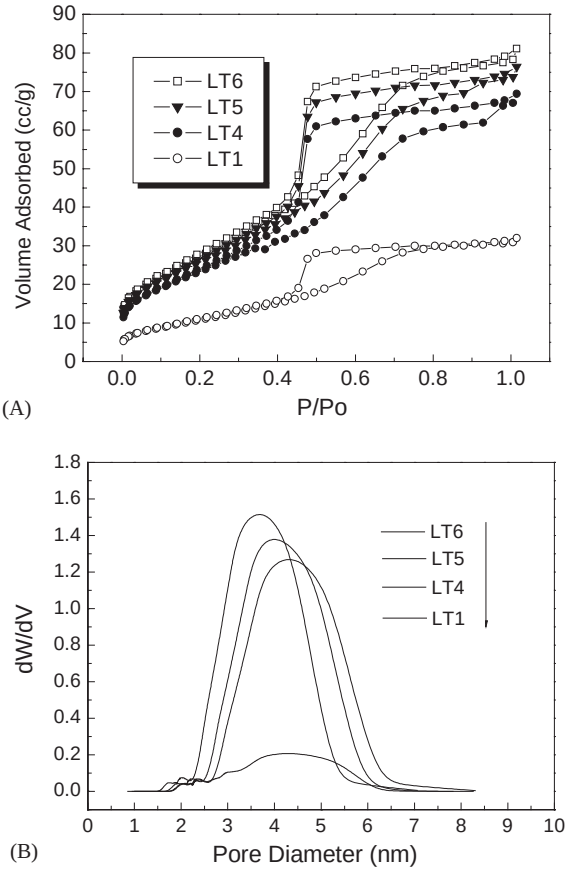

Fig. 6. (A–B) Nitrogen adsorption–desorption isotherm and pore size distributions of LT1, LT5, LT6 and LT7 calcinated at 700°C for 1 h at the same heating condition.

doped samples calcined at 500°C and 700°C as show in Table 2. Compared to the pure TiO_2, the pore size of lanthanum-doped titania is shifted to the smaller size at 500°C. When the temperature elevated to 700°C, it was not possible to distinguish peaks in the pore size distribution curves of pure TiO_2. Moreover, an average pore size around 4 nm for LT4, LT5, and LT6 can still be observed (Fig. 6B). The pore size distribution of LT1 (0.25%) is greatly broadened compared to the higher lanthanum content samples. These results show that the lanthanum doping into the titania is able to stabilize their textural structures, arrest their agglomeration, and maintain the mesopores. The other lanthanide dopants show the similar effect.

The photoactivity of as-prepared lanthanide-doped titania was detected by the degradation of Rhodamine B aqueous solution under UV irradiation. Fig. 7 presents the photocatalytic activities of lanthanum-, gadolinium-, and ytterbium-doped samples calcined at 500°C as the

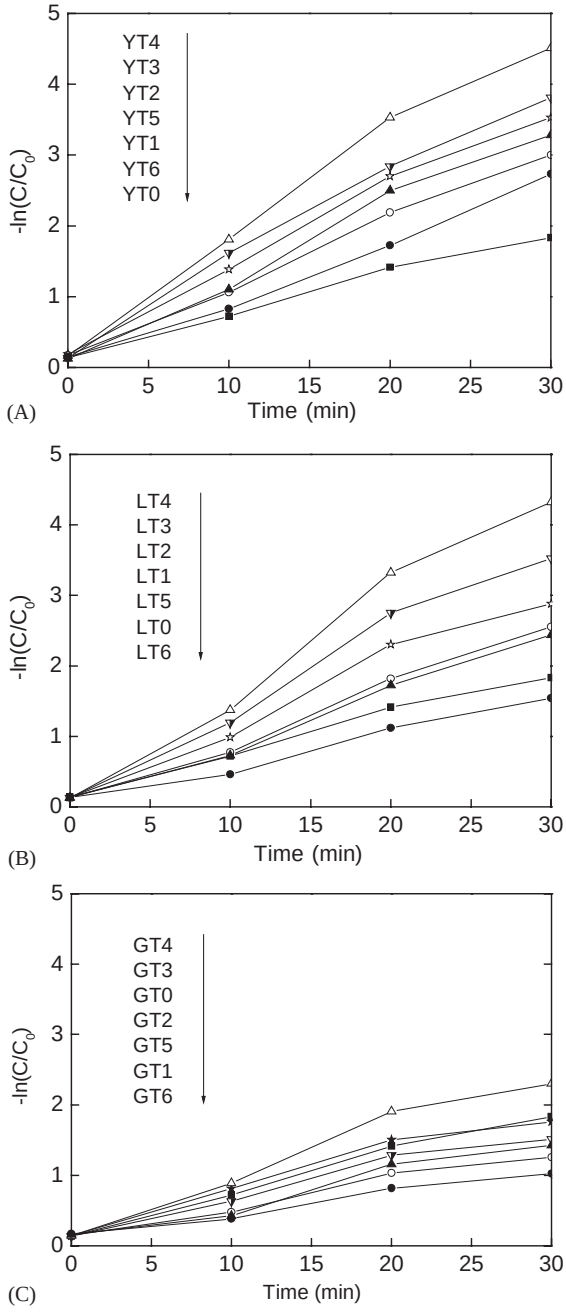

Fig. 7. The photocatalytic properties of titania-doped different lanthanide content calcined at 500°C for 1 h in air. C_0 is the initial concentration of RB (10^{-5} M) and C is the concentration after irradiation. (A) ytterbium-doped titania; (B) lanthanum-doped titania; (C) gadolinium-doped titania.

degradation of RB, $-\ln(C/C_0)$, versus time. It is seen that the photoreactivity of ytterbium-doped TiO_2 is increased significantly compared to the undoped titania (Fig. 7A). The highest photoreactivity is generated by the 2 at% ytterbium-doped sample (Fig. 7A, YT4), which causes 97% Rhodimine B to be degraded after 30 min irradiation. The photoactivity shows a steady decrease with the further increase of the ytterbium content, although the photoreactivity of per individual ytterbium-doped TiO_2 is still higher than undoped TiO_2. According to the results of Tables 1 and 2 and TEM (Fig. 5), the agglomeration and sintering of lanthanide-doped TiO_2 is effectively restrained by the lanthanide dopants and thus the higher concentration doped TiO_2 shows the less particle size and higher surface area. The photoreactivity enhancement of the ytterbium-doped TiO_2 cannot be ascribed to a simple increase in reactive surface area because the samples over the concentration of 2% lose their reactivity gradually. Ranjit et al. [32] recently concluded that the enhancement of photoactivity for lanthanide-doped titania is attributed to the concentrated organic materials at the semiconductor surface by the formation of complex between the doped lanthanide ions and substrates. The ability of lanthanides to form complexes with various Lewis bases such as amines, alcohols has been used in NMR spectroscopy where the magnetic features of lanthanide ions yield significant chemical shifts in the protons associated these organic ligands. Our results are in general agreement with the conclusion. The doped samples show the enhanced photoreactivity when compared with undoped TiO_2. However our results also reveal that the improved activity is not proportional with the lanthanide concentration and a maximum was observed for 2% doped titania (YT4). Theoretically speaking, the greater amount of lanthanide ion should be favorable to the more complex formation, and thus the enhanced activity should be observed with higher lanthanide content samples. Therefore, the concentration of substrate at the TiO_2 semiconductor surface by forming complex is likely not the only factor that influences the activity. The manner in existence of Ln^{3+} may also play an important role in the activity of the lanthanide-doped titania. The lanthanide dopants in TiO_2 should have two existing manners: one is the replacement of Ti^{4+} site to form Ti–O–*Ln* bond in the lattice. The other is in the interstitial because of the mismatch of the ionic sizes of Ln^{3+} and Ti^{4+} (Ln^{3+} is much larger than Ti^{4+}). The properties of interstitial Ln^{3+} ions should be more similar with that in oxide lanthanide, and it is known that the oxide lanthanides themselves show no photocatalytic properties to the degradation of RB. In contrast, the properties of lanthanide ions forming Ti–O–*Ln* bond should be greatly changed and should exert a great influence to the activity of titania. The observation of a maximum value for the photocatalysis of various lanthanide content doped titania will be reasonable if we suppose that the kind of replacement of Ti^{4+} by Ln^{3+} is saturated at a certain level, like the occasions of crystalline titanium silicalites TS-1 [40].

In the case of lanthanum doping, the photoreactivity of doped samples is generally improved by lanthanum doping and the activity maximum is seen for the 2% lanthanum-doped TiO_2 (LT4) (Fig. 7B), showing the similar reactivity variation trend to ytterbium-doped samples over the same time scale. The efficiencies of gadolinium as dopants with respect to photoreactivity are substantially different from lanthanum and ytterbium, even though La^{3+}, Yb^{3+}, and Gd^{3+} belong to lanthanide family and have identical oxidation states. Most of gadolinium-doped samples show the lower activity than undoped TiO_2 (Fig. 7C). The highest photoreactivity, however, is still observed for the 2% gadolinium-doped titania (GT4), which exhibits an enhanced photoreactivity compared to undoped TiO_2. The photocatalysis behavior of gadolinium dopants may be related to its electronic configuration. It is reported that the stability of a closed electronic shell makes the hole/electron trapping unfavorable, and metal ions as dopants in TiO_2 with a close-shell electronic configuration had little effect on the photoreactivity of TiO_2 [22,41]. The low photoreactivity of gadolinium-doped TiO_2 is probably attributed to the stable partly closed electronic configuration of Gd^{3+} ($4f^7$).

We examined the activities of samples calcined at 900°C for 1 h. It is found that the activity is reduced considerably for the samples calcined at 900°C. Exploring the XRD reflections of lanthanide-doped titania calcined at 900°C (Figs. 1B, 2B and 3B), both rutile and lanthanide titanium oxide modification were evolved and their intensity was progressively strengthened with the increase of lanthanide content. Together with the diminution of surface areas, the rapid transition of A-R and the formation of lanthanide titanium oxide probably bring about the rapid activity reduction of samples caicined at 900°C.

4. Conclusions

The phase transformation, thermal stability, and photoactivity of lanthanide-doped nanosized mesoporous titania were studied. The rare earth doping was found to be able to significantly inhibit the A-R phase transformation, stabilize the mesoporous structure, and retard the diminishing of surface area of nanosized TiO_2 at high temperatures. It is demonstrated that the A-R phase transformation in lanthanide-doped titania is sensitive to the radius of lanthanide. The lanthanide with a larger atom/ion radius shows the stronger inhibitory effect to the A-R transition of TiO_2. The stability of mesoporous structure of TiO_2 is significantly

improved by lanthanide dopants. It is worthy noting that the radius of the lanthanide is of great influence to the development of lanthanide titanium oxide in TiO_2 at high temperature. Lanthanides with larger atom/ion radius show preference to form higher coordination number lanthanide titanium oxide. Significantly improved photocatalytic behavior is observed for lanthanum- and ytterbium-doped titania.

Acknowledgments

Y.H. Zhang acknowleges Prof. A.Reller for his discussions. This work was financed by Natural Science Foundation of China (No. 20373061) and Natural Science Foundation of Zhejiang Province, China (No. 202035).

References

[1] A. Fujishima, K. Hashimoto, T. Watanabe, TiO_2 Photocatalysis Fundamentals and Applications, BKC Inc., Tokyo, 1999.
[2] M.R. Hoffmann, S.T. Martin, W.Y. Choi, D.W. Bahnemann, Chem. Rev. 95 (1995) 69.
[3] B. O'Regan, M. Grätzel, Nature 353 (1991) 737.
[4] M.A. Fox, M.Y. Dulay, Chem. Rev. 93 (1993) 341.
[5] Song, et al., Metals Mater. Int. 8 (1) (2002) 103–109.
[6] Arbiol, et al., J. Appl. Phys. 92 (2002) 853.
[7] S. Karvinen, Solid State Sci. 5 (2003) 811.
[8] R.J. Berry, M.R. Mueller, Microchem. J. 50 (1994) 28.
[9] J. Augustynski, Electrochim. J. 38 (1993) 43.
[10] M. Graezel, Prog. Photovoltaics 8 (2000) 172.
[11] S. Rajeshkumar, C. Suresh, A.K. Vasudevan, N.R. Suja, P. Mukundan, K.G.K. Warrier, Mater. Lett. 38 (1999) 161.
[12] D. Vorkapic, T. Matscukas, J. Am. Ceram. Soc. 81 (1998) 2815.
[13] H. Zhang, J.F. Banfield, J. Mater. Res. 15 (2000) 437.
[14] J. Soria, J.C. Conesa, V. Augugliaro, L. Palmisano, M. Schiavello, A. Sclafani, J. Phys. Chem. 95 (1991) 274.
[15] M.I. Litter, J.A. Navio, J. Photochem. Photobiol. A 98 (1996) 171.
[16] P.O. Larsson, A. Andersson, Appl. Catal. B 24 (2000) 175.
[17] K.E. Karakitsou, X.E. Verykios, J. Phys. Chem. 97 (1993) 1184.
[18] S.T. Martin, C.L. Morrison, M.R. Hoffmann, J. Phys. Chem. 98 (1994) 13695.
[19] H. Schneider, A. Baiker, V. Schar, A. Waukaun, J. Catal. 146 (1994) 545.
[20] J. Yang, J.M.F. Ferreira, Mater. Lett. 36 (1998) 320.
[21] (a) Y.H. Zhang, A. Reller, J. Mater. Chem. 11 (2001) 2537;
(b) Y.H. Zhang, S. Ebbinghaus, A. Weidenkaff, A. Reller, T. Kurz, H.A.K. Nidda, P.J. Klar, M. Güngerich, Chem. Mater. 15 (2003) 4028.
[22] W. Choi, A. Termin, M.R. Hoffmann, J. Phys. Chem. 98 (1994) 13669.
[23] R. Abe, K. Sayama, H. Arakawa, Chem. Phys. Lett. 371 (2003) 360.
[24] W. Choi, A. Termin, M.R. Hoffmann, Angew. Chem., Int. Ed. Engl. 33 (1994) 1091.
[25] T. López, J. Hernandez-Ventura, R. Gómez, F. Tzompantzi, E. Sánchez, X. Bokhimi, A. Garcýá, J. Mol. Catal. A: Chem. 167 (2001) 101.
[26] K.N.P. Kumar, A. Burggraaf, J. Mater. Chem. 3 (1993) 141.
[27] R. Gopalan, Y.S. Lin, Ind. Eng. Chem. Res. 34 (1995) 1189.
[28] G. Boschloo, A. Hagfeldt, Chem. Phys. Lett. 370 (2003) 381.
[29] D.J. Bjorkert, R. Mayappan, D. Holland, M.H. Lewis, J. Eur. Ceram. Soc. 19 (1999) 1847.
[30] M.S.P. Francisco, V.R. Mastelaro, Chem. Mater. 14 (2002) 2514.
[31] C.P. Sibu, K.S. Rajesh, P. Mukundan, K.G.K. Warrier, Chem. Mater. 14 (2002) 2876.
[32] K.T. Ranjit, I. Willner, S.H. Bossmann, A.M. Braun, Environ. Sci. Technol. 35 (2001) 1544.
[33] J. Lin, J.C. Yu, J. Photochem. Photobiol. A: Chem. 116 (1998) 63.
[34] D.W. Hwang, J.S. Lee, W. Li, S.H. Oh, J. Phys. Chem. B 107 (2003) 4963.
[35] Y.H. Zhang, H.X. Zhang, Y.X. Xu, Y.G. Wang, J. Mater. Chem. 13 (2003) 2261.
[36] C. Anderson, A.L. Bard, J. Phys. Chem. B 101 (1997) 2611.
[37] Y.H. Zhang, A. Reller, Mater. Lett. 57 (2003) 4108.
[38] H. Klug, L. Alexander, X-ray Diffraction Procedures, Wiley, New York, 1962.
[39] K.S. Sing, D.H. Everett, R.A.W. Haul, L. Moscou, R.A. Pierotti, J. Rouquerol, T. Siemieniewska, Pure Appl. Chem. 57 (1985) 603.
[40] M. Taramasso, G. Perego, B. Notari, US Patent4 410 (1983) 501.
[41] P.A. Cox, Transition Metal Oxides: An Introduction to their Electronic Structure and Properties, Clarendon Press, Oxford, 1992.